


Cite this: *RSC Adv.*, 2020, 10, 35889

# Study on the unsteady state oxidative coupling of methane: effects of oxygen species from O<sub>2</sub>, surface lattice oxygen, and CO<sub>2</sub> on the C<sub>2+</sub> selectivity†

Suji Yoon,<sup>‡ab</sup> Seoyeon Lim,<sup>‡ab</sup> Jae-Wook Choi,<sup>a</sup> Dong Jin Suh,<sup>ac</sup> Kwang Ho Song<sup>id bc</sup> and Jeong-Myeong Ha<sup>id \*acd</sup>

This study examined the effects of oxygen species on the unsteady-state oxidative coupling of methane (OCM) using a lengthy catalyst bed of Na<sub>2</sub>WO<sub>4</sub>/Mn/SiO<sub>2</sub>. The reaction conditions, including the methane-to-oxygen ratio, ratio of feed gas dilution by N<sub>2</sub>, quantity of catalyst, and feed flow rate were adjusted for the continuous flow fixed bed reaction system. While the O<sub>2</sub> gas initiated methyl radical formation from methane, the surface lattice oxygen atoms improved the dehydrogenation of paraffins to olefins without significant activation of methane. The addition of CO<sub>2</sub> as a mild oxidizing agent was also tested and slightly improved OCM selectivity with slightly lower methane conversion were observed.

Received 11th July 2020  
Accepted 17th September 2020

DOI: 10.1039/d0ra06065h

rsc.li/rsc-advances

## 1. Introduction

The vast reserves of natural and shale gas have led to global interest in converting methane, their major component, to valuable chemicals. The oxidative coupling of methane (OCM) can directly produce ethylene using oxidizing agents including oxygen gas at a high reaction temperature (>600 °C), and hence it is a promising way to use the highly stable methane as feedstock. The proposed mechanism for OCM is composed of parallel and consecutive heterogeneous and gas-phase reactions.<sup>1</sup> The catalyst surface activated by the co-fed oxygen produces methyl radicals by hydrogen abstraction from methane. The methyl radicals can then be converted to the desired ethane in the gas phase, or further oxidized to the undesired CO and CO<sub>2</sub>. It was suggested that an industrially feasible OCM process can be developed if the C<sub>2+</sub> products (hydrocarbons containing two or more carbon atoms) achieve a yield above 25% and a selectivity of 75–80%.<sup>2–9</sup>

Because there is a critical technological barrier for the selective formation of olefins and paraffins while suppressing

the deep oxidation of methane to CO and CO<sub>2</sub>,<sup>6,8,10</sup> many selective oxidation catalysts have been prepared for the OCM reaction. For unpromoted oxides of alkali, alkaline-earth, and rare earth metals, low CH<sub>4</sub> conversion and high C<sub>2+</sub> selectivities were observed, along with lower C<sub>2+</sub> yields (<12%),<sup>11</sup> although moderate OCM activity was achieved at lower reaction temperatures (<750 °C).<sup>12</sup> Perovskites, which are well-defined crystalline mixed oxides containing two different metals, were also used for catalyzing OCM,<sup>13–15</sup> exhibiting improved activity with promoter addition.<sup>1,12</sup> Among them, Na<sub>2</sub>WO<sub>4</sub>/Mn/SiO<sub>2</sub> is one of the most effective and stable OCM catalysts.<sup>9,16–21</sup> An optimized catalyst, composed of 2 wt% Mn and 5 wt% Na<sub>2</sub>WO<sub>4</sub> on SiO<sub>2</sub>, has exhibited ~25% C<sub>2+</sub> yield.<sup>6</sup> The remarkable long-term stability of Na<sub>2</sub>WO<sub>4</sub>/Mn/SiO<sub>2</sub> (1000 h) was also reported for continuous-flow reactions.<sup>21</sup> Although the origin of its high catalytic activity has not yet been elucidated,<sup>22</sup> the unusual formation of α-cristobalite SiO<sub>2</sub> phase during calcination at 750–850 °C has been reported as a distinguishing feature of a good catalyst,<sup>23</sup> and the active species has been suggested to be Na<sup>+</sup> or Na<sub>2</sub>WO<sub>4</sub> on silica surface with distorted WO<sub>4</sub><sup>2–</sup> tetrahedra formed during phase transition.<sup>23–25</sup> In addition to the roles played by Na<sub>2</sub>WO<sub>4</sub>, manganese oxide was reported to improve the oxygen mobility *via* reduction of Mn<sup>3+</sup> to Mn<sup>2+</sup>.<sup>26</sup> Because of the proposed oxygen activation by Mn in the Na–O–Mn composites,<sup>27</sup> the selective formation of ethylene, which can occur by oxidative or non-oxidative dehydrogenation of ethane, can be controlled by tuning the surface Mn concentration.<sup>24,28</sup> Improved OCM activity by the addition of several additives to Na<sub>2</sub>WO<sub>4</sub>/Mn/SiO<sub>2</sub> has also been reported.<sup>9,29</sup>

Although a number of selective catalysts have been developed, a better understanding of the reaction conditions is also

<sup>a</sup>Clean Energy Research Centre, Korea Institute of Science and Technology, Seoul 02792, Republic of Korea. E-mail: jmha@kist.re.kr

<sup>b</sup>Department of Chemical and Biological Engineering, Korea University, Seoul 02841, Republic of Korea

<sup>c</sup>Graduate School of Energy and Environment (Green School), Korea University, Seoul 02841, Republic of Korea

<sup>d</sup>Division of Energy and Environment Technology, KIST School, Korea University of Science and Technology, Seoul 02792, Republic of Korea

† Electronic supplementary information (ESI) available. See DOI: 10.1039/d0ra06065h

‡ These authors equally contributed to this work.



required to achieve a feasible OCM process. Because of the limited supply of  $O_2$  and the high  $CH_4$  conversion through the reactor, in which a reactant mixture flows downward through the catalyst bed, the conditions including reactant compositions in the upper catalyst bed may be significantly different from those in the lower catalyst bed. When methane and oxidant are flown through the oxygen-rich top bed, the oxidant (mostly  $O_2$ ) can be adsorbed on the catalyst surface. The adsorbed oxygen species activates methane by abstracting H to form methyl radicals, which are coupled to form ethane. In the oxygen-deficient bottom layer, methyl radicals,  $C_{2+}$  products, and carbon oxides are present and can interact with the unreacted methane and oxidant. The unreacted  $O_2$  can activate methane by either forming methyl radical or deeply oxidize the highly active  $C_{2+}$  products to CO and  $CO_2$ , thereby decreasing the  $C_{2+}$  selectivity. The amount of initially supplied oxidants also influences the level of deep oxidation products in the bottom layer.

By using less-active oxidizing agents, including  $H_2O$  and  $CO_2$ , the selectivity of OCM products can be improved by suppressing the burning of valuable hydrocarbons to form CO and  $CO_2$ .<sup>30</sup> Water as an oxidant improved the coupling selectivity over perovskite catalysts, exhibiting increased  $C_2$  production with increasing partial pressure of steam.<sup>31</sup>  $CO_2$  has also been suggested as an alternative oxidant to  $O_2$ .<sup>32–37</sup> The formation of surface lattice oxygen atoms from  $CO_2$  has been observed on  $PbO$ - $MgO$  and  $PbO$ - $CaO$  catalysts, which improves the abstraction of hydrogen atoms from methane.<sup>32,35</sup> In  $Na_2WO_4/Mn/SiO_2$ , the presence of  $CO_2$  caused structural modification to improve catalytic activity.<sup>38</sup> The formation of hot spots, which accelerate the deep oxidation to CO and  $CO_2$  because of significant local exothermic reaction, was observed in the catalyst bed of a bench-scale OCM reactor,<sup>39</sup> and these hot spots can be reduced by the presence of  $CO_2$  with high heat capacity.<sup>40</sup> In addition to the improved OCM activity, the presence of  $CO_2$  stabilized the lithium-doped  $MgO$  catalyst and suppressed its deactivation.<sup>36</sup> For oxidative dehydrogenation, it was suggested that  $CO_2$  improves selective OCM and stabilizes the catalysts by poisoning the nonselective active sites.<sup>41</sup>

The goal of this study is to understand the local OCM reaction throughout the catalyst bed under continuously changing reaction conditions, which can be attributed to the limited supply of oxidizing reagents (particularly  $O_2$ ) in the fixed bed system. The temperature (750–850 °C),  $N_2$  dilution ratio,  $CH_4/O_2$  ratio, catalyst bed thickness, total feed flow rate, and the co-feeding rate of  $CO_2$  were varied to study the behaviors of reactants and products under these continuously changing conditions. The effects of  $O_2$  and  $CO_2$  (as strong and mild oxidizing reagent, respectively) on the local OCM reaction were investigated in a long fixed bed system, which is meant to simulate possible scaled-up reactors.  $CO_2$  as a mild oxidizing reagent can also function as a diluent in the OCM process, and it can be recycled with the unreacted methane in the industrial scale process. With continuous consumption of  $O_2$  throughout the long catalyst bed and the formation of  $O_2$ -deficient region, the roles of lattice oxygen atoms on the OCM were also observed. Although a steady state was not achieved while the lattice

oxygen atoms were being consumed for the OCM, the unsteady state reaction examined here is useful for understanding the OCM reaction using lattice oxygen atoms. The spent catalysts were characterized using X-ray diffraction (XRD), X-ray photoelectron spectroscopy (XPS), and Raman spectroscopy to reveal changes in the catalysts during the OCM reaction.

## 2. Experimental

### 2.1. Materials

All chemicals were used without further purification. Sodium tungstate dihydrate ( $Na_2WO_4 \cdot 2H_2O$ , 99+%) was purchased from Yakuri Pure Chemicals (Kyoto, Japan). Manganese nitrate hexahydrate ( $Mn(NO_3)_2 \cdot 6H_2O$ , 98%) was purchased from Kanto Chemical (Tokyo, Japan). Silica gel ( $SiO_2$ , 60–325 mesh, 99.5%) was purchased from Johnson Matthey (Royston, United Kingdom). Manganese(II) tungsten oxide ( $MnWO_4$ , 99.9%) was purchased from Alfa Aesar (Haverhill, Massachusetts, USA). Manganese(III) oxide ( $Mn_2O_3$ , 99.9%) was purchased from Sigma-Aldrich (St. Louis, Missouri, USA). Methane ( $CH_4$ , 99.95%), oxygen ( $O_2$ , 99.995%), nitrogen ( $N_2$ , 99.9%), and carbon dioxide ( $CO_2$ , 99.99%) were purchased from Shinyang Sanso (Seoul, Korea). DI water (18.2 MΩ m) was prepared using an aquaMAX-Ultra 370 series water purification system (Young Lin Instruments, Anyang, Korea).

### 2.2. Catalyst preparation

The catalyst containing 5 wt%  $Na_2WO_4$  and 2 wt% Mn on  $SiO_2$  ( $Na_2WO_4/Mn/SiO_2$ ) was prepared using a mixed slurry method.<sup>39,42</sup> Silica gel (28 g) was mixed with DI water (150 mL) and stirred at 105 °C for 1 h under reflux.  $Mn(NO_3)_2 \cdot 6H_2O$  (3.146 g) dissolved in DI water (10 mL) and  $Na_2WO_4 \cdot 2H_2O$  (1.684 g) dissolved in DI water (10 mL) were added drop-wise to the boiling mixture using a syringe pump over 15 min. The prepared thick paste was dried in air at 105 °C for 16 h and then calcined in air at 800 °C for 5 h. Prior to the reaction, the prepared catalyst powder was passed through 70–140 mesh.

### 2.3. Catalytic activity measurement

The catalytic reaction was performed using a fixed bed cylindrical quartz reactor (ID = 6 mm, length = 370 mm) (Fig. S1†). The unreacted  $O_2$  leaving the catalyst bed can contribute to further homogeneous oxidation of the  $C_{2+}$  products to CO and  $CO_2$  before the product mixture was inactivated by cooling,<sup>38</sup> which hinders interpretation of the reaction results. To reduce homogeneous reaction of the product mixture, a narrow exit was introduced on the reactor to encourage its fast outflow. The outlet of the reactor was narrower than the inlet (1 vs. 6 mm). The catalyst bed was located at the center of the reactor, with quartz wool placed at its upper and lower ends.  $ZrSiO_4$  beads (Cenotec, Co. Ltd.) were positioned on the top of the catalyst bed to minimize the homogeneous reactions. A reaction mixture of  $CH_4$ ,  $O_2$ ,  $N_2$ , and  $CO_2$  flowed into the catalyst bed. Notably, the furnace temperature, which was used as the reaction temperature in this study, was controlled (Fig. S2†). The measured temperature of catalyst bed was 0–40 °C higher, depending on the position in the



catalyst bed and the reaction conditions. The temperature measured at the bottom of catalyst bed was closest to the furnace temperature. Because the change of temperature through the catalyst bed was similar at each reaction temperature, we used the furnace temperature as the reaction temperature for convenience. Gas hourly space velocity (GHSV) was adjusted using catalyst bed volume and reactant flow rate. Water formed during the OCM reaction was removed at a cold trap ( $-2\text{ }^{\circ}\text{C}$ ) connected to a chiller (VTRC-620, Jeio Tech). After an hour of isothermal operation, the product mixture was collected and analyzed using a thermal conductivity detector (TCD) and a flame ignition detector (FID) installed onto an online-gas chromatography system (Agilent 7890A).  $\text{CH}_4$ ,  $\text{O}_2$ ,  $\text{N}_2$ ,  $\text{CO}$ , and  $\text{CO}_2$  were analyzed using the TCD with a Carboxen 1000 column (Supelco, 60–80 mesh,  $4.6\text{ m} \times 1/8\text{ in} \times 2.1\text{ mm}$ ), and the hydrocarbons were analyzed using the FID with an HP-PLOT  $\text{Al}_2\text{O}_3$  S capillary column ( $50\text{ m} \times 320\text{ }\mu\text{m} \times 8\text{ }\mu\text{m}$ ). The catalytic performance was characterized by the following parameters:

$$\text{CH}_4 \text{ conversion } (X(\text{CH}_4), \%) = \frac{\text{moles of CH}_4 \text{ consumed}}{\text{moles of CH}_4 \text{ in the feed}} \times 100$$

$$\text{Selectivity to compound i } (S(i), \%) = \frac{\text{number of carbon atoms per compound i molecule} \times \text{moles of compound i}}{\text{moles of CH}_4 \text{ consumed}} \times 100$$

$$\text{C}_{2+} \text{ selectivity } (S(\text{C}_{2+}), \%) = \frac{2 \times \text{moles of C}_2 \text{ hydrocarbons} + 3 \times \text{moles of C}_3 \text{ hydrocarbons}}{\text{moles of CH}_4 \text{ consumed}} \times 100$$

$$\text{O}_2 \text{ conversion } (X(\text{O}_2), \%) = \frac{\text{moles of O}_2 \text{ consumed}}{\text{moles of O}_2 \text{ in the feed}} \times 100$$

$$\text{C}_{2+} \text{ yield } (Y(\text{C}_{2+}), \%) = \frac{\text{CH}_4 \text{ conversion} \times \text{C}_{2+} \text{ selectivity}}{100}$$

Table 1 Reactions during the OCM process

Reaction
CO production: $\text{CH}_4 + \frac{3}{2}\text{O}_2 \rightarrow \text{CO} + 2\text{H}_2\text{O}$
$\text{CO}_2$ production: $\text{CH}_4 + 2\text{O}_2 \rightarrow \text{CO}_2 + 2\text{H}_2\text{O}$
$\text{C}_2\text{H}_6$ production: $\text{CH}_4 + \frac{1}{4}\text{O}_2 \rightarrow \frac{1}{2}\text{C}_2\text{H}_6 + \frac{1}{2}\text{H}_2\text{O}$
$\text{C}_2\text{H}_4$ production: $\text{CH}_4 + \frac{1}{2}\text{O}_2 \rightarrow \frac{1}{2}\text{C}_2\text{H}_4 + \text{H}_2\text{O}$
$\text{C}_3\text{H}_8$ production: $\text{CH}_4 + \frac{1}{3}\text{O}_2 \rightarrow \frac{1}{3}\text{C}_3\text{H}_8 + \frac{2}{3}\text{H}_2\text{O}$
$\text{C}_3\text{H}_6$ production: $\text{CH}_4 + \frac{1}{2}\text{O}_2 \rightarrow \frac{1}{3}\text{C}_3\text{H}_6 + \text{H}_2\text{O}$

$$\text{Olefins/paraffins}(\text{mol/mol}) =$$

$$\frac{\text{moles of ethylene and propylene produced}}{\text{moles of ethane and propane produced}}$$

$\text{O}_2$ -consumption for product i, the fraction of  $\text{O}_2$  in the feed required to convert  $\text{CH}_4$  into each product component i, was obtained using the following relationship described in Table 1:

## 2.4. Catalyst characterization

XRD results were collected to observe the catalysts' crystal structures using a Shimadzu XRD-6000 device equipped with a  $\text{CuK}\alpha_1$  ( $\lambda = 0.15406\text{ nm}$ ) source. Raman spectroscopy analysis was performed using a Renishaw InVia Raman microscope. The surface electronic structures were analyzed using a PHI 5000 Versa Probe X-ray photoelectron spectroscope at Korea Basic Science Institute (Busan, Korea). The XPS spectra were calibrated using C 1s peak at  $284.6\text{ eV}$ .

$$\text{O}_2\text{-consumption for compound i } (\text{O}_2\text{-cons.}(i), \%) =$$

$$\frac{S(i) \times \text{moles of O}_2 \text{ molecules to convert CH}_4 \text{ to compound i}}{S(\text{CO}) \times \frac{3}{2} + S(\text{CO}_2) \times 2 + S(\text{C}_2\text{H}_6) \times \frac{1}{4} + S(\text{C}_2\text{H}_4) \times \frac{1}{2} + S(\text{C}_3\text{H}_8) \times \frac{1}{3} + S(\text{C}_3\text{H}_6) \times \frac{1}{2}} \times 100$$



### 3. Results and discussion

#### 3.1. Effects of CH<sub>4</sub>/O<sub>2</sub> ratio and N<sub>2</sub> dilution on catalysis

Before investigating the effects of reaction conditions on the OCM results, the effects of O<sub>2</sub> concentration or the CH<sub>4</sub>/O<sub>2</sub> ratio on the OCM activity were studied. CH<sub>4</sub>/O<sub>2</sub> = 3 mol/mol was selected as an optimal reaction condition in this study because of the high C<sub>2+</sub> selectivity with moderate CH<sub>4</sub> conversion, although the highest C<sub>2+</sub> yield was not achieved using this ratio (Fig. 1 and Table S1†). Notably, in this study, C<sub>2+</sub> compounds include ethane, ethylene, propane, and propylene. When CH<sub>4</sub>/O<sub>2</sub> was adjusted from 1 to 6 mol/mol at 800 °C, the highest C<sub>2+</sub> yield of 21.5% (44.0% CH<sub>4</sub> conversion and 49.0% C<sub>2+</sub> selectivity) was achieved at 800 °C when CH<sub>4</sub>/O<sub>2</sub> = 2 mol/mol. The C<sub>2+</sub> selectivity sharply increased with increasing CH<sub>4</sub>/O<sub>2</sub> ratio up to 3 mol/mol, and then steadily increased. Based on these observations, we selected CH<sub>4</sub>/O<sub>2</sub> = 3 mol/mol for the good CH<sub>4</sub> conversion and high C<sub>2+</sub> selectivity. The observed increase in C<sub>2+</sub> selectivity and decrease in CH<sub>4</sub> conversion at a higher CH<sub>4</sub>/O<sub>2</sub> ratio (*i.e.*, reducing the limited supply of oxygen reactant) were consistent with the results of previous studies.<sup>43</sup> At higher CH<sub>4</sub>/O<sub>2</sub> ratios, the amount of O<sub>2</sub> was insufficient for activating the large number of methane molecules, thus the CH<sub>4</sub> conversion decreased. At lower CH<sub>4</sub>/O<sub>2</sub> ratios, the formation of methyl radicals was improved by the high partial pressure of O<sub>2</sub> to achieve high CH<sub>4</sub> conversion, but the methyl radicals were also easily oxidized to CO and CO<sub>2</sub> to decrease the C<sub>2+</sub> yield (Table S1†). These observations suggest that a moderate CH<sub>4</sub>/O<sub>2</sub> ratio is required to achieve a high C<sub>2+</sub> yield by combining the CH<sub>4</sub> conversion and C<sub>2+</sub> selectivity.

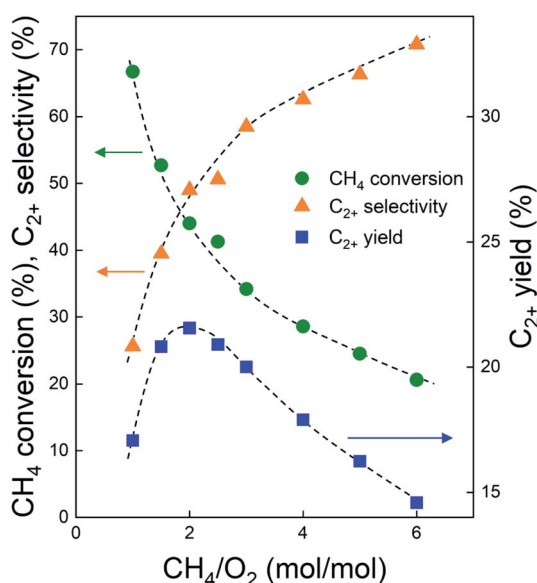


Fig. 1 CH<sub>4</sub> conversion (circles), C<sub>2+</sub> selectivity (triangles), and C<sub>2+</sub> yield (rectangles) over Na<sub>2</sub>WO<sub>4</sub>/Mn/SiO<sub>2</sub> catalyst at 800 °C and different CH<sub>4</sub>/O<sub>2</sub> (mol/mol) ratios. The O<sub>2</sub> conversions were 100% for all cases. GHSV = 10 000 h<sup>-1</sup>. CH<sub>4</sub> flow rate was fixed at 18 mL min<sup>-1</sup>, and the flow rates of O<sub>2</sub> and N<sub>2</sub> were adjusted to achieve the total flow rate of 50 mL min<sup>-1</sup>.

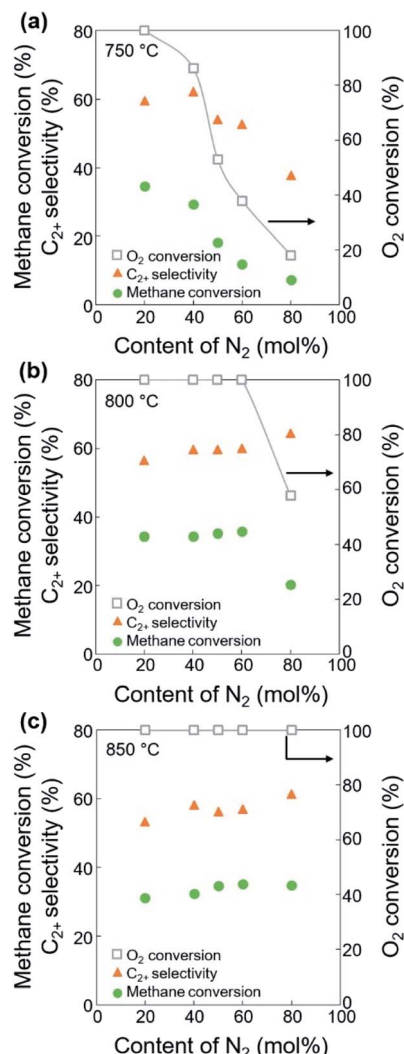


Fig. 2 CH<sub>4</sub> conversion (circles), C<sub>2+</sub> selectivity (triangles), and O<sub>2</sub> conversion (squares) using different contents of N<sub>2</sub> diluent at (a) 750 °C, (b) 800 °C, and (c) 850 °C. CH<sub>4</sub>/O<sub>2</sub> ratio = 3 mol/mol, GHSV = 10 000 h<sup>-1</sup>.

With the CH<sub>4</sub>/O<sub>2</sub> ratio fixed at 3 mol/mol, an optimized N<sub>2</sub> dilution ratio of 20% (v/v) or CH<sub>4</sub>/O<sub>2</sub>/N<sub>2</sub> = 3/1/1 mol/mol/mol produced the best CH<sub>4</sub> conversion and C<sub>2+</sub> selectivity (Fig. 2 and Table S2†). High concentrations of methane and O<sub>2</sub> can accelerate the reaction rates, and the deep oxidation of methane to CO and CO<sub>2</sub> may occur along with the formation of hot spots because of the large heat of reaction.<sup>39</sup> Diluting the reactant mixture decreases the partial pressures of methane and O<sub>2</sub> and thus improves the selectivity for coupled C<sub>2+</sub> hydrocarbons while suppressing the formation of CO and CO<sub>2</sub>.<sup>39,44,45</sup> This change in the OCM results was more significant at the higher temperatures of 800–850 °C (with CH<sub>4</sub> conversions > 20%) and less significant at 750 °C (with CH<sub>4</sub> conversions < 20%). When the feed was highly diluted at the low reaction temperature, the formed methyl radicals may not be able to undergo gas-phase coupling with other methyl radicals in the highly diluted environment, which may reduce the C<sub>2+</sub> selectivity. The general





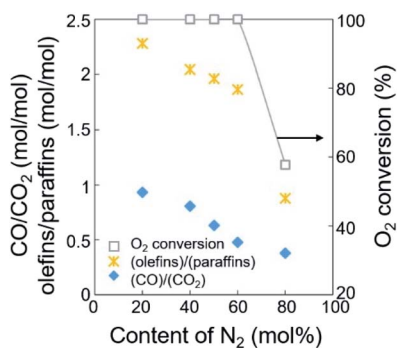


Fig. 3 Ratios of olefins/paraffins and CO/CO<sub>2</sub> for the dehydrogenation of paraffins and the oxidation of CO, depending on the content of N<sub>2</sub> diluent at 800 °C.

trend of increasing C<sub>2+</sub> selectivity with increasing CH<sub>4</sub> conversion, under different reaction conditions for the same catalysts, has also been observed in our previous studies.<sup>46–48</sup>

The ratios of CO/CO<sub>2</sub> and olefins/paraffins increased at lower dilution by N<sub>2</sub> or higher partial pressures of the reactants (Fig. 3, S3, and Table S2†). Because higher partial pressures of the reactants are expected to improve the formation of CO<sub>2</sub> and increase the olefins/paraffins ratio,<sup>44</sup> the improved formation of CO rather than CO<sub>2</sub> we observed must come from another reaction pathway, which will be discussed later in the Section 3.2. Note that the amount of O<sub>2</sub> required for forming CO<sub>2</sub> is 1.33 times larger than that for forming CO, and the production of olefins from methane requires more than twice the amount of O<sub>2</sub> required to produce paraffins. Because of the limited supply of O<sub>2</sub> in this study, the deep oxidation to CO and CO<sub>2</sub> consumed more O<sub>2</sub> and suppressed the methane activation and the dehydrogenation, and this lowered the olefins/paraffins ratio.

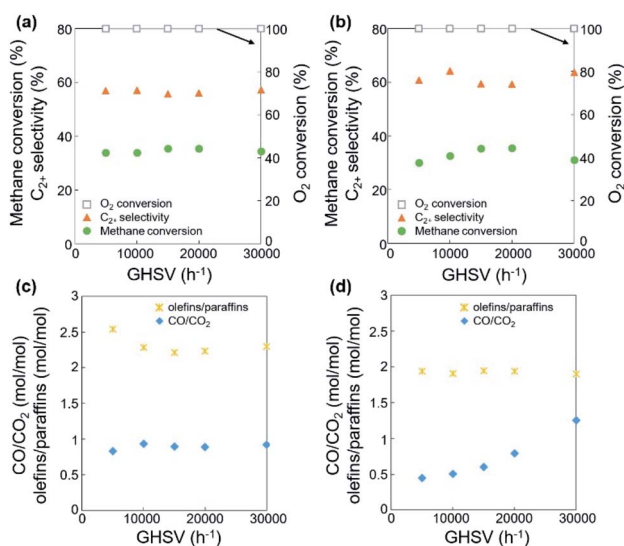


Fig. 4 (a and b) Catalytic activities and (c and d) ratios of olefins/paraffins and CO/CO<sub>2</sub> for the dehydrogenation of paraffins and the oxidation of CO, depending on the catalyst bed thickness (a and c) and feed flow rate (b and d) at 800 °C.

### 3.2. Effects of catalyst bed thickness and feed flow rate on catalysis

Using the fixed CH<sub>4</sub>/O<sub>2</sub> ratio and N<sub>2</sub> dilution, the effects of oxygen species on the OCM activity were investigated. The oxygen species activating methane and other hydrocarbons change throughout the long catalyst bed at a fixed flow rate. Both O<sub>2</sub> gas and surface oxygen species contribute to OCM, while only the latter are present at the O<sub>2</sub>-deficient bottom part of the bed. With increasing catalyst bed thickness and the same flow rates of reactants, along with increasing residence time and decreasing GHSV, the reaction results did not significantly change when the O<sub>2</sub> was completely converted (Fig. 4a, c, S4, Tables S3 and S4†). While incomplete conversion of O<sub>2</sub> was observed at lower GHSV and lower reaction temperature, the 100% O<sub>2</sub> conversion produced almost the same CH<sub>4</sub> conversion (32.1–35.9%) along with 50.9–59.8% C<sub>2+</sub> selectivity and 16.8–20.5% C<sub>2+</sub> yield. The negligible C<sub>2+</sub> production and CH<sub>4</sub> conversion in the O<sub>2</sub>-deficient region (when 100% O<sub>2</sub> conversion was reached) indicated that the O<sub>2</sub> gas was required for significant conversion of methane to the C<sub>2+</sub> compounds. Compared to the smaller changes in CH<sub>4</sub> conversion and C<sub>2+</sub> selectivity, the olefin selectivity increased with increasing catalyst bed thickness, indicating that the olefins were formed by the oxidative dehydrogenation of paraffins at the O<sub>2</sub>-deficient region. Based on these observations, the oxidative dehydrogenation of paraffins to olefins can be initiated by the surface lattice oxygen atoms. In contrast, the production of methyl radicals that contributed to CH<sub>4</sub> conversion was less initiated by these surface lattice oxygen atoms because there was no significant increase of CH<sub>4</sub> conversion at the O<sub>2</sub>-deficient region. Therefore, the surface lattice oxygen atoms, which were formed by diffusion of bulk lattice oxygen atoms to the catalyst surface, mainly dehydrogenated the paraffins to olefins. Meanwhile, the surface-adsorbed oxygen atoms from the bulk O<sub>2</sub> gas preferentially converted methane to methyl radicals, which were further coupled to produce paraffins. In addition to the formation of olefins, the production of CO<sub>2</sub> also slightly increased with increasing catalyst bed thickness, indicating that dehydrogenation using surface lattice oxygen species was accompanied by deep oxidation to form CO<sub>2</sub> as by-product.

The OCM was also studied at a fixed catalyst bed thickness (0.18 mL or 6.4 mm) and adjustable feed flow rates (15–90 mL min<sup>−1</sup>) to confirm the role of each oxygen species at CH<sub>4</sub>/O<sub>2</sub>/N<sub>2</sub> = 3/1/1 mol/mol/mol (Fig. 4b, d, S5, Tables S5 and S6†). When 100% O<sub>2</sub> conversion was achieved, the CH<sub>4</sub> conversion (28.5–35.5%) and C<sub>2+</sub> selectivity (56.5–64.2%) were not significantly adjusted at 800–850 °C, indicating no significant dependence of OCM activity on the feed flow rate.

While the dehydrogenation of paraffins to olefins occurred at the O<sub>2</sub>-deficient region using surface lattice oxygen species, as depicted in Fig. 4 and Table S3,† decreasing the feed flow rate, which has the same effect as increasing the catalyst bed thickness at a the fixed flow rate, did not significantly affect the dehydrogenation activity (Table S5†). A turbulent flow in the catalyst bed may suppress formation of the O<sub>2</sub>-deficient region, obscuring the effects of surface lattice oxygen species.



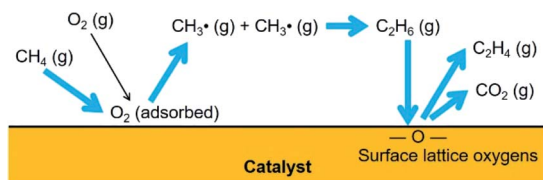


Fig. 5 Reactions by oxygen species.

In addition to dehydrogenation, the preferred formation of  $\text{CO}_2$  over  $\text{CO}$  was observed, which indicates deeper oxidation to  $\text{CO}_2$  at a lower GHSV, lower feed flow rate, or longer residence time. Particularly at  $850^\circ\text{C}$ , the  $\text{CO}/\text{CO}_2$  ratio significantly decreased at lower feed flow rate or longer residence time (Table S5†). The improved formation of  $\text{CO}_2$ , which consumed a large quantity of oxygen species, also reduced the  $\text{CH}_4$  conversion because of the lack of oxidizing reagents. The preferred formation of  $\text{CO}$  at a shorter residence time can be attributed to the gas-phase formation of  $\text{CO}$  from methyl radicals.<sup>5,49</sup>  $\text{CO}$  can be preferentially produced when a methyl radical reacts with  $\text{O}_2$  instead of another methyl radical, increasing the  $\text{CO}/\text{CO}_2$  ratio.

The reactions preferred by the adsorbed  $\text{O}_2$  and the surface lattice oxygen species are depicted in Fig. 5. Methane molecules were activated by the surface-adsorbed  $\text{O}_2$  to form methyl radicals, which were then coupled to ethane. Ethane molecules were oxidatively dehydrogenated by the surface lattice oxygen species to form ethylene. The activation of methane molecules to methyl radicals by the surface lattice oxygen species was negligible; however, the dehydrogenation of paraffins and deep oxidation of hydrocarbons can be preferred by the surface lattice oxygen species.

### 3.3. Effects of the catalyst bed thickness on the catalysis with co-fed $\text{CO}_2$

Based on the improved formation of  $\text{CO}_2$  at lower feed flow rates, we studied the effects of a mild oxidant such as  $\text{CO}_2$  on the OCM selectivity (or the product distributions of paraffins, olefins,  $\text{CO}$ , and  $\text{CO}_2$ ). As one of the products of OCM,  $\text{CO}_2$  can act as a diluent or a mild oxidant replacing the diluent  $\text{N}_2$  and the oxidant  $\text{O}_2$ .<sup>36,38,50</sup> As a mild oxidant, a moderate concentration of  $\text{CO}_2$  has been reported to improve the  $\text{C}_{2+}$  selectivity and reduce the  $\text{CH}_4$  conversion.<sup>38,51,52</sup> For example,  $\text{MgO}$  or  $\text{Sm}_2\text{O}_3$ -based catalysts exhibited increased  $\text{C}_{2+}$  selectivity with a low partial pressure of  $\text{CO}_2$ .<sup>32,53</sup> Suppressed OCM activity with  $\text{CO}_2$  has also been reported:  $\text{Li}/\text{MgO}$  was poisoned by  $\text{CO}_2$ ,<sup>54</sup> and  $\text{Na}_2\text{WO}_4/\text{Mn}/\text{SiO}_2$  was deactivated by concentrated  $\text{CO}_2$ .<sup>38</sup> Nevertheless, it may be possible to modify the OCM activity by using an appropriate amount of co-fed  $\text{CO}_2$  as mild oxidant to replace the mixture of  $\text{N}_2$  and  $\text{O}_2$ . Thus, the OCM reaction was tested at a fixed feed flow rate, variable catalyst bed thickness, and the 20%  $\text{N}_2$  in the feed was replaced by 16%  $\text{CO}_2$  + 4%  $\text{N}_2$  in order to investigate this possibility and understand the effects of the adsorbed oxygen atoms (Fig. 6, S6, Tables S7 and S8†).

When increasing the catalyst bed thickness (or decreasing the GHSV),  $\text{CH}_4$  conversion and  $\text{C}_{2+}$  selectivity reached 30.8–34.5% and 51.1–61.9%, respectively at 100%  $\text{O}_2$  conversion

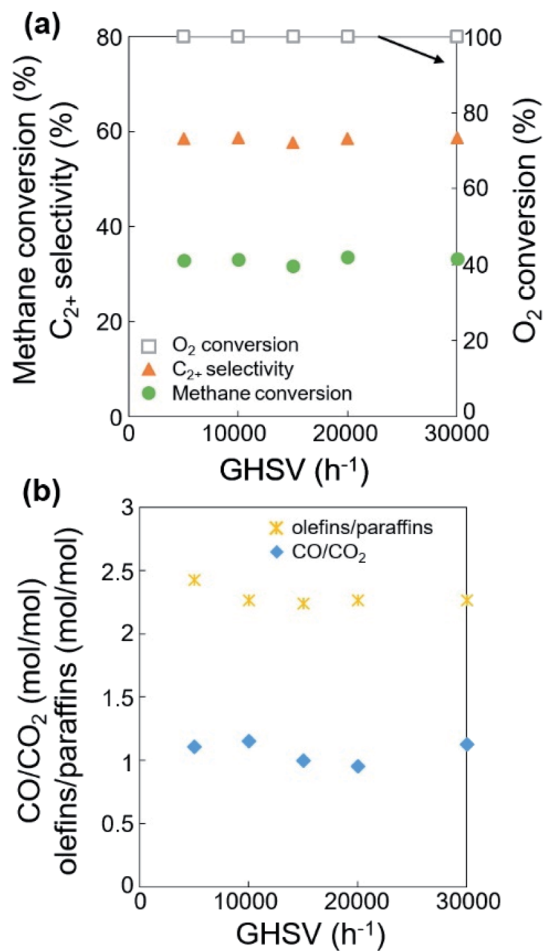


Fig. 6 (a) Catalytic activities, (b) ratios of olefins/paraffins and  $\text{CO}/\text{CO}_2$ , and (c) oxygen consumption for the dehydrogenation of ethane (or propane) and the oxidation of  $\text{CO}$ , depending on the catalyst bed thickness at  $\text{CH}_3/\text{O}_2/\text{N}_2/\text{CO}_2 = 3/1/0.2/0.8$  mol/mol/mol/mol and  $800^\circ\text{C}$ .

(Table S5†), which is similar to the results using  $\text{N}_2$  as diluent (32.1–35.9% and 50.9–59.8%, respectively, Table S3†). Compared with the use of  $\text{N}_2$  diluent, the co-feeding of  $\text{CO}_2$  slightly lowered  $\text{CH}_4$  conversion and slightly improved  $\text{C}_{2+}$  selectivity by 1.5–4.7%, achieving almost identical  $\text{C}_{2+}$  yields. The improved  $\text{C}_{2+}$  selectivity was more distinct when the  $\text{O}_2$  was not completely consumed ( $\text{O}_2$  conversion < 100%), particularly when  $\text{GHSV} > 20\,000\text{ h}^{-1}$  at  $750^\circ\text{C}$ .

In terms of the selectivity between  $\text{CO}$  and  $\text{CO}_2$ , a larger  $\text{CO}/\text{CO}_2$  ratio was observed when  $\text{CO}_2$  was co-fed compared to using the  $\text{N}_2$  diluent alone (Tables S3 and S7†). The improved formation of  $\text{CO}$  with  $\text{CO}_2$  co-feeding can be attributed to the catalytic conversion of  $\text{CO}_2$  to  $\text{CO}$ . While this conversion can occur by either the reduction or catalytic dissociation of  $\text{CO}_2$ , a highly oxidizing environment can suppress the reduction reaction by hydrogen generated in the dehydrogenation of paraffin or reduction of water. The catalytic dissociation of  $\text{CO}_2$  to  $\text{CO}$  and  $\text{O}$  may occur to increase the concentration of  $\text{CO}$ ,<sup>50,51</sup> and the produced oxygen atoms may improve the  $\text{C}_{2+}$  selectivity.

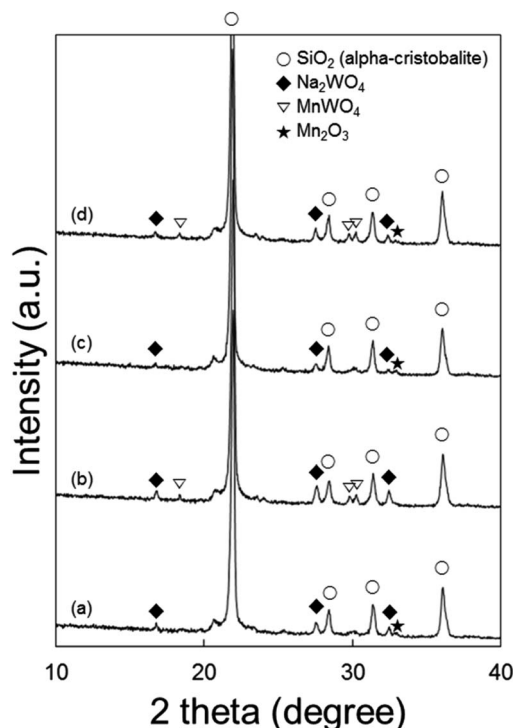


Fig. 7 XRD results of Na<sub>2</sub>WO<sub>4</sub>/Mn/SiO<sub>2</sub> spent in the reaction with N<sub>2</sub> diluent from the (a) top and (b) bottom of the catalyst bed, and in the reaction with co-fed CO<sub>2</sub> from the (c) top and (d) bottom of the catalyst bed. The peaks were assigned to α-cristobalite SiO<sub>2</sub> (○), Na<sub>2</sub>WO<sub>4</sub> (◆), MnWO<sub>4</sub> (▽), and Mn<sub>2</sub>O<sub>3</sub> (★).

The actual temperatures of the top, middle, and bottom layers of the 35.3 mm catalyst bed were measured (Fig. S2†). The temperature was observed to decrease from the top to the bottom layer, indicating that the involved reactions occurred at the entrance of the catalyst bed.

We also summarized all the reaction results obtained in this study in terms of C<sub>2+</sub> yield, depending on CH<sub>4</sub> conversion and O<sub>2</sub> conversion (Fig. S7†). Regardless of reaction conditions, CH<sub>4</sub> conversion, O<sub>2</sub> conversion (for <100%), and C<sub>2+</sub> yield increased proportionally with each other, indicating that the formation of C<sub>2+</sub> compounds was not significantly adjusted by varying the reaction conditions, as long as O<sub>2</sub> was present. Thus, the effects of surface lattice oxygen species may not be significant while O<sub>2</sub> is present.

### 3.4. Identification of crystal structures

To understand the effects of catalyst structures on the OCM activity, the spent catalysts were characterized (Fig. 7). There was no significant difference between catalysts spent using N<sub>2</sub> as diluent alone and with CO<sub>2</sub> co-feeding. However, when using a longer catalyst bed or smaller GHSV, catalysts on the top and bottom of the bed exhibited different structures. The formation of MnWO<sub>4</sub> was distinct at the bottom (O<sub>2</sub>-deficient region) but not clearly observed at the top (O<sub>2</sub>-rich region). While MnWO<sub>4</sub> had been reported in the literature as either an active or inactive component,<sup>22,28,47,55,56</sup> we observed moderate OCM activity on

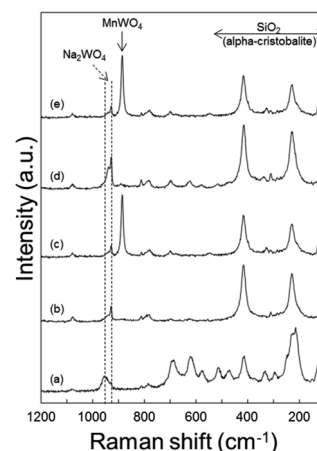


Fig. 8 Raman spectra of Na<sub>2</sub>WO<sub>4</sub>/Mn/SiO<sub>2</sub> catalyst: (a) in the fresh state, after the reaction with N<sub>2</sub> diluent at the (b) top and (c) bottom of the catalyst bed, after the reaction with co-fed CO<sub>2</sub> at the (d) top and (e) bottom of the catalyst bed.

MnWO<sub>4</sub> powder (Fig. S9†). While the co-existing Na<sub>2</sub>WO<sub>4</sub> and α-cristobalite SiO<sub>2</sub> are known as key components for good OCM catalysts,<sup>22,23,57</sup> it is not clear whether the formation of MnWO<sub>4</sub> reduced the OCM activity or not in this study.

When heated to 800 °C in air, the Na<sub>2</sub>WO<sub>4</sub> and Mn<sub>2</sub>O<sub>3</sub> phases were found to disappear for the fresh catalyst at room temperature, indicating the melting of these solid materials (Fig. S8(a)†). Compared to these, MnWO<sub>4</sub> survived, while maintaining its solid structure at the OCM reaction temperature. α-Cristobalite SiO<sub>2</sub> exhibited a peak shift toward smaller 2θ or larger *d*-spacings, indicating thermal expansion of the crystal structure.

### 3.5. Study of catalyst surface by Raman spectroscopy and XPS

Raman spectra of the spent catalysts also confirmed the formation of MnWO<sub>4</sub> in the O<sub>2</sub>-deficient region (bottom layer of catalyst bed) by the distinct MnWO<sub>4</sub> peak at 885 cm<sup>-1</sup> for both CO<sub>2</sub>-free and CO<sub>2</sub>-added feeds (Fig. 8). Raman bands indicating Na<sub>2</sub>WO<sub>4</sub> were observed in the fresh catalyst and spent ones at all regions of the bed. Notably, the bands at or below 500 cm<sup>-1</sup> can be attributed to α-cristobalite SiO<sub>2</sub>, and those at 500–700 cm<sup>-1</sup> can be attributed to manganese oxides.<sup>24</sup> When heated to 800 °C in air, Mn<sub>2</sub>O<sub>3</sub> and α-cristobalite SiO<sub>2</sub> peaks became weaker than those of the fresh catalyst, indicating that these phases became weaker or less ordered at high temperatures (Fig. S8(b)†).

In terms of surface electronic structures, the spent catalysts exhibited more intense Na 1s and Mn 2p peaks when only N<sub>2</sub> was used as diluent in the reaction (Table S9†). The O 1s peaks at 530.9 eV indicating the presence of Na<sub>2</sub>WO<sub>4</sub> were stronger than those with co-fed CO<sub>2</sub> (Fig. S10†). The peaks at 532.6 eV are assigned to SiO<sub>2</sub>. Compared to the fresh catalyst, the spent catalysts after reaction with N<sub>2</sub> as the only diluent or with co-fed CO<sub>2</sub> had much higher surface concentrations of Mn as measured by XPS (Table S9†). This growing surface concentration of Mn can be attributed to the formation of MnWO<sub>4</sub>, even



Table 2 OCM results using spent catalyst prepared in the O<sub>2</sub>-deficient region (bottom of catalyst bed)<sup>a,b</sup>

Reaction temperature (°C)	X(CH <sub>4</sub> ) (%)	X(O <sub>2</sub> ) (%)	S(C <sub>2+</sub> ) (%)	Y(C <sub>2+</sub> ) (%)	Olefins/paraffins (mol mol <sup>-1</sup> )
<b>Fresh Na<sub>2</sub>WO<sub>4</sub>/Mn/SiO<sub>2</sub></b>					
750	35.2	100	54.5	19.2	2.12
800	35.3	100	51.5	18.2	2.49
850	33.4	100	45.9	15.4	3.77
<b>Spent Na<sub>2</sub>WO<sub>4</sub>/Mn/SiO<sub>2</sub> prepared in the O<sub>2</sub>-deficient region</b>					
750	35.0	98.2	59.6	20.8	2.11
800	35.8	100	53.4	19.1	2.68
850	34.1	100	49.9	17.0	3.98

<sup>a</sup> GHSV = 10 000 h<sup>-1</sup>, CH<sub>4</sub>/O<sub>2</sub>/N<sub>2</sub> = 3/1/1 mol/mol/mol, total feed flow rate = 30 mL min<sup>-1</sup>. <sup>b</sup> X(CH<sub>4</sub>): CH<sub>4</sub> conversion, X(O<sub>2</sub>): O<sub>2</sub> conversion, S(C<sub>2+</sub>): C<sub>2+</sub> selectivity, Y(C<sub>2+</sub>): C<sub>2+</sub> yield.

though the distinct peaks could not be identified because the Mn may have protruded to the surface by complexation with W species.<sup>47</sup>

The spent catalyst from the O<sub>2</sub>-deficient region (which exhibited the formation of MnWO<sub>4</sub>) was re-used for the OCM, and the activity was compared with the fresh one (Table 2). The spent catalyst exhibited higher C<sub>2+</sub> selectivity, higher C<sub>2+</sub> yield, and higher olefins/paraffins ratio by 3.7–9.4%, 4.9–10.4%, and 0–7.6%, respectively. Therefore, the spent catalysts containing MnWO<sub>4</sub> produced more C<sub>2+</sub> compounds along with a higher dehydrogenation activity. These observations confirmed that dehydrogenation occurred preferably in the O<sub>2</sub>-deficient region, which exhibited the formation of MnWO<sub>4</sub>.

## 4. Conclusions

The catalytic oxidative coupling of methane to C<sub>2+</sub> compounds was examined under various reaction conditions, and the following results were obtained.

(i) Oxygen species formed by the adsorption of gas-phase O<sub>2</sub> preferentially activated methane molecules to produce methyl radicals, while those formed by the diffusion of bulk lattice oxygen atoms preferred the dehydrogenation of paraffins to olefins.

(ii) The co-feeding of CO<sub>2</sub> slightly increased the C<sub>2+</sub> selectivity compared to the reaction without CO<sub>2</sub> co-feeding; however, no significant improvement was observed exhibiting almost identical C<sub>2+</sub> yield, although beneficial effects have been reported.

(iii) The formation of MnWO<sub>4</sub> on the catalyst was improved in the O<sub>2</sub>-free environment at the O<sub>2</sub>-deficient bottom of the catalyst bed, which exhibited the preferred dehydrogenation reaction. This also confirmed the diffusion of bulk lattice oxygen atoms to the catalyst surface.

In this study, we focused on the OCM reaction in the non-steady states. The roles of surface lattice oxygen atoms and the reaction-initiated changes in the catalyst bed were clearly observed. Those results will help researchers and engineers understand the scaled-up OCM processes for the conversion of methane to paraffins and olefins.

## Conflicts of interest

There are no conflicts to declare.

## Acknowledgements

This research was supported by C1 Gas Refinery Program through the National Research Foundation of Korea (NRF) funded by the Ministry of Science and ICT (2015M3D3A1A01064900).

## Notes and references

- 1 S. Lim, J.-W. Choi, D. J. Suh, K. H. Song, H. C. Ham and J.-M. Ha, *J. Catal.*, 2019, **375**, 478–492.
- 2 B. L. Farrell, V. O. Igenegbai and S. Linic, *ACS Catal.*, 2016, **6**, 4340–4346.
- 3 J. C. W. Kuo, C. T. Kresge and R. E. Palermo, *Catal. Today*, 1989, **4**, 463–470.
- 4 A. M. Maitra, *Appl. Catal., A*, 1993, **104**, 11–59.
- 5 J. H. Lunsford, *Angew. Chem., Int. Ed.*, 1995, **34**, 970–980.
- 6 U. Zavyalova, M. Holena, R. Schlogl and M. Baerns, *ChemCatChem*, 2011, **3**, 1935–1947.
- 7 Y. S. Su, J. Y. Ying and W. H. Green, *J. Catal.*, 2003, **218**, 321–333.
- 8 A. Cruellas, J. J. Bakker, M. V. Annaland, J. A. Medrano and F. Gallucci, *Energy Convers. Manage.*, 2019, **198**, 111789.
- 9 N. S. Hayek, G. J. Khelif, F. Horani and O. M. Gazit, *J. Catal.*, 2019, **376**, 25–31.
- 10 S. Arndt, G. Laugel, S. Levchenko, R. Horn, M. Baerns, M. Scheffler, R. Schlögl and R. Schomäcker, *Catal. Rev.*, 2011, **53**, 424–514.
- 11 J. M. DeBoy and R. F. Hicks, *Ind. Eng. Chem. Res.*, 1988, **27**, 1577–1582.
- 12 S. Lim, J.-W. Choi, D. Jin Suh, U. Lee, K. H. Song and J.-M. Ha, *Catal. Today*, 2020, **352**, 127–133.
- 13 G. Lee, I. Kim, I. Yang, J.-M. Ha, H. B. Na and J. C. Jung, *Appl. Surf. Sci.*, 2018, **429**, 55–61.
- 14 D. Kwon, I. Yang, Y. Sim, J.-M. Ha and J. C. Jung, *Catal. Commun.*, 2019, **128**, 105702.





- 15 Y. Sim, J. Yoo, J.-M. Ha and J. C. Jung, *J. Energy Chem.*, 2019, **35**, 1–8.
- 16 S.-B. Li, *Chin. J. Chem.*, 2001, **19**, 16–21.
- 17 U. Simon, O. Gorke, A. Berthold, S. Arndt, R. Schomacker and H. Schubert, *Chem. Eng. J.*, 2011, **168**, 1352–1359.
- 18 S. Pak and J. H. Lunsford, *Appl. Catal., A*, 1998, **168**, 131–137.
- 19 H. R. Godini, A. Gili, O. Gorke, U. Simon, K. Hou and G. Wozny, *Energy Fuels*, 2014, **28**, 877–890.
- 20 V. Fleischer, R. Steuer, S. Parishan and R. Schomacker, *J. Catal.*, 2016, **341**, 91–103.
- 21 S. Li, *J. Nat. Gas Chem.*, 2003, **12**, 1–9.
- 22 S. Arndt, T. Otremba, U. Simon, M. Yildiz, H. Schubert and R. Schomäcker, *Appl. Catal., A*, 2012, **425–426**, 53–61.
- 23 A. Palermo, J. P. Holgado Vazquez, A. F. Lee, M. S. Tikhov and R. M. Lambert, *J. Catal.*, 1998, **177**, 259–266.
- 24 S.-F. Ji, T.-C. Xiao, S.-B. Li, C.-Z. Xu, R.-L. Hou, K. S. Coleman and M. L. H. Green, *Appl. Catal., A*, 2002, **225**, 271–284.
- 25 J. G. Wu and S. B. Li, *J. Phys. Chem.*, 1995, **99**, 4566–4568.
- 26 Y. Kou, B. Zhang, J.-z. Niu, S.-b. Li, H.-l. Wang, T. Tanaka and S. Yoshida, *J. Catal.*, 1998, **173**, 399–408.
- 27 D. J. Wang, M. P. Rosynek and J. H. Lunsford, *J. Catal.*, 1995, **155**, 390–402.
- 28 S. Ji, T. Xiao, S. Li, L. Chou, B. Zhang, C. Xu, R. Hou, A. P. E. York and M. L. H. Green, *J. Catal.*, 2003, **220**, 47–56.
- 29 S. Gu, H. S. Oh, J. W. Choi, D. J. Suh, J. Jae, J. Choi and J. M. Ha, *Appl. Catal., A*, 2018, **562**, 114–119.
- 30 J. S. Chang, V. P. Vislovskiy, M. S. Park, D. Y. Hong, J. S. Yoo and S. E. Park, *Green Chem.*, 2003, **5**, 587–590.
- 31 X. H. Li, K. Tomishige and K. Fujimoto, *Catal. Lett.*, 1996, **36**, 21–24.
- 32 T. Nishiyama and K.-I. Aika, *J. Catal.*, 1990, **122**, 346–351.
- 33 C. L. Chen, Y. D. Xu, G. J. Li and X. X. Guo, *Catal. Lett.*, 1996, **42**, 149–153.
- 34 S. Alzahrani, Q. Song and L. L. Lobban, *Ind. Eng. Chem. Res.*, 1994, **33**, 251–258.
- 35 K.-i. Aika and T. Nishiyama, *J. Chem. Soc., Chem. Commun.*, 1988, 70–71, DOI: 10.1039/C39880000070.
- 36 S. J. Korf, J. A. Roos, N. A. de Bruijn, J. G. van Ommen and J. R. H. Ross, *J. Chem. Soc., Chem. Commun.*, 1987, 1433–1434, DOI: 10.1039/C39870001433.
- 37 J. Shi, L. Yao and C. W. Hu, *J. Energy Chem.*, 2015, **24**, 394–400.
- 38 J. Shi, L. Yao and C. Hu, *J. Energy Chem.*, 2015, **24**, 394–400.
- 39 J. Y. Lee, W. Jeon, J.-W. Choi, Y.-W. Suh, J.-M. Ha, D. J. Suh and Y.-K. Park, *Fuel*, 2013, **106**, 851–857.
- 40 R. M. Freire, F. F. de Sousa, A. L. Pinheiroa, E. Longhinotti, J. Mendes, A. C. Oliveira, P. D. C. Freire, A. P. Ayala and A. C. Oliveira, *Appl. Catal., A*, 2009, **359**, 165–179.
- 41 J. S. Yoo, P. S. Lin and S. D. Elflin, *Appl. Catal., A*, 1993, **106**, 259–273.
- 42 J. Wang, L. Chou, B. Zhang, H. Song, J. Zhao, J. Yang and S. Li, *J. Mol. Catal. A: Chem.*, 2006, **245**, 272–277.
- 43 V. O. Igenegbai, R. J. Meyer and S. Linic, *Appl. Catal., B*, 2018, **230**, 29–35.
- 44 T. P. Tiemersma, M. J. Tuinier, F. Gallucci, J. A. M. Kuipers and M. v. S. Annaland, *Appl. Catal., A*, 2012, **433–434**, 96–108.
- 45 M. R. Lee, M. J. Park, W. Jeon, J. W. Choi, Y. W. Suh and D. J. Suh, *Fuel Process. Technol.*, 2012, **96**, 175–182.
- 46 W. Jeon, J. Y. Lee, M. Lee, J.-W. Choi, J.-M. Ha, D. J. Suh and I. W. Kim, *Appl. Catal., A*, 2013, **464–465**, 68–77.
- 47 R. T. Yunarti, S. Gu, J.-W. Choi, J. Jae, D. J. Suh and J.-M. Ha, *ACS Sustainable Chem. Eng.*, 2017, **5**, 3667–3674.
- 48 S. Gu, H.-S. Oh, J.-W. Choi, D. J. Suh, J. Jae, J. Choi and J.-M. Ha, *Appl. Catal., A*, 2018, **562**, 114–119.
- 49 C. Karakaya, H. Y. Zhu, C. Loebick, J. G. Weissman and R. J. Kee, *Catal. Today*, 2018, **312**, 10–22.
- 50 T. Yabe and Y. Sekine, *Fuel Process. Technol.*, 2018, **181**, 187–198.
- 51 Y. Liu, J. Xue, X. Liu, R. Hou and S. Li, in *Stud. Surf. Sci. Catal.*, ed. D. S. F. F. A. V. A. Parmaliana and F. Arena, Elsevier, 1998, vol. 119, pp. 593–597.
- 52 Y. Liu, R. L. Hou, X. X. Liu, J. Z. Xue and S. B. Li, in *Natural Gas Conversion V*, ed. A. Parmaliana, D. Sanfilippo, F. Frusteri, A. Vaccari and F. Arena, Elsevier Science Publ B V, Amsterdam, 1998, vol. 119, pp. 307–311.
- 53 S. Kuś, M. Otremba, A. Tórz and M. Taniowski, *Appl. Catal., A*, 2002, **230**, 263–270.
- 54 K. P. Peil, J. G. Goodwin Jr and G. Marcelin, *J. Catal.*, 1991, **131**, 143–155.
- 55 S. Sadjadi, S. Jaso, H. R. Godini, S. Arndt, M. Wollgarten, R. Blume, O. Gorke, R. Schomacker, G. Wozny and U. Simon, *Catal. Sci. Technol.*, 2015, **5**, 942–952.
- 56 T. W. Elkins and H. E. Hagelin-Weaver, *Appl. Catal., A*, 2015, **497**, 96–106.
- 57 Z. C. Jiang, C. J. Yu, X. P. Fang, S. B. Li and H. L. Wang, *J. Phys. Chem.*, 1993, **97**, 12870–12875.

